Transportation Research Interdisciplinary Perspectives 34 (2025) 101733

Contents lists available at ScienceDirect

Transportation Research Interdisciplinary Perspectives

journal homepage: www.elsevier.com/locate/trip

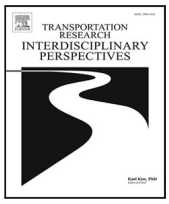

Investigating comfort-oriented optimization of eco-driving cruising strategy: A driving simulator study

Haoxiang Xue, Federico Maria Ballo, Giorgio Previati *, Gianpiero Mastinu, Massimiliano Gobbi

Department of Mechanical Engineering, Politecnico di Milano, Via La Masa 1, Milan, 20156, Italy

ARTICLE INFO

Keywords:
Eco-driving strategy
Pulse and glide
Multi-objective optimization
Jerk threshold
Ride comfort
Driving simulator

ABSTRACT

Eco-driving cruising strategies can effectively reduce energy demand and contribute to extend the range of full electric vehicles. However, the adoption of these strategies, involving alternating cycles of acceleration and deceleration as a replacement for constant-speed cruising, may potentially compromise the longitudinal comfort of the vehicle. In this paper, a method for a comfort-oriented optimization of eco-driving cruising strategies is proposed and validated by using a dynamic driving simulator. Dynamic driving simulators are rarely used for longitudinal comfort assessment. Therefore, a series of preliminary tests are conducted to compare the longitudinal comfort perceived on a driving simulator and on an actual vehicle. It turns out that, with appropriate cueing settings, the perceived longitudinal comfort remains consistent across both scenarios. Moreover, levels of jerk related to the perception of vehicle comfort at different velocities are identified to serve as reference in the eco-driving strategy design. On the basis of these results, an eco-driving cruising strategy is optimized within a two-step multi-objective framework based on GA by considering both energy consumption and longitudinal comfort. Subsequently, the Pareto points corresponding to the thresholds, representing the occupants' comfort preferences, are evaluated at the driving simulator. These tests show that the comfort ranking of the solution is consistent between the optimization process and the subjective perceptions and confirm the reference jerk levels determined in the preliminary tests and the effectiveness of the optimization procedure, indicating dynamic driving simulators can be effectively employed to assess the longitudinal comfort of vehicles and to evaluate eco-driving cruising strategies.

1. Introduction

Eco-driving strategies refer to a set of driving practices and techniques aimed at minimizing fuel consumption, reducing emissions and promoting environmental friendly transportation. In order to maintain the powertrain system working at high efficiency, repeated acceleration and coasting is a widely employed strategy. The pulse and glide (PnG) strategy, alternating the vehicle between "pulse" (accelerating) and "glide" (coasting), is one of the classic driving strategies using this approach. Compared with the most frequently used cruising strategy, the constant speed (CS) strategy, the PnG strategy can achieve more fuel/energy savings by optimizing the phases of pulse and glide (Lee, 2009). In addition, the PnG shows an excellent potential for reducing the fuel consumption in the speed range between 5 m/s to 35 m/s, and can achieve the best fuel-saving performance (about 32% reduction of fuel consumption with respect to the CS strategy) at 15 m/s in a car-following scenario (Li and Peng, 2012).

Smart and electric vehicles are acknowledged as a sustainable personal mobility system, especially in urban environments (Faria et al., 2012, 2019). The application of PnG strategies and adaptive cruise control (ACC) to EVs has also attracted wide attention. Referring to ultra-efficient lightweight EVs specifically designed for mileage competitions (Stabile et al., 2021), the optimization of eco-driving strategies has been extensively discussed in several papers (Targosz et al., 2018; Olivier et al., 2017; Ballo et al., 2022). For passenger vehicles, the PnG strategy has been considered to be the most effective (Kim and Ahn, 2019). However, in most cases the strategy is optimized offline leading to a loss of optimality when actually employed. A real-time control structure is proposed in Kim and Ahn (2019) for online PnG optimization. In Shieh et al. (2023), an online implementable MPC controller for the PnG strategy is proposed, for an hybrid vehicle, to balance both fuel economy and ride comfort while maintaining the state of charge (SOC) in a car-following scenario.

* Corresponding author.
E-mail address: giorgio.previati@polimi.it (G. Previati).

https://doi.org/10.1016/j.trip.2025.101733
Received 16 April 2025; Received in revised form 24 October 2025; Accepted 7 November 2025
Available online 11 November 2025
2590-1982/© 2025 The Authors. Published by Elsevier Ltd. This is an open access article under the CC BY license (http://creativecommons.org/licenses/by/4.0/).

Eco-driving strategies involve a driving style that differs from what is typically expected by drivers and passengers, for example, incorporating a series of accelerations and decelerations in situations where a constant speed would normally be anticipated. From both social and personal perspectives, the acceptance of such driving styles needs to be evaluated (Muehlbacher et al., 2023). This is particularly important in the case of automated vehicles (AVs), where acceptance plays a crucial role. To this end, the driving style of AVs must be comfortable (Peng et al., 2024).

Ride comfort, defined as the level of comfort experienced by occupants during vehicle traveling, is another critical aspect of vehicle performance (Heißing and Ersoy, 2010). With the development of AVs and advanced driver assistance systems (ADAS), the driving styles for passenger comfort has gained significant attention (Peng et al., 2024; Jungblut et al., 2023). Frequent accelerations and decelerations of the PnG strategy may cause discomfort (Sohn et al., 2020). Comfort assessment, however, is inherently subjective (Heißing and Ersoy, 2010). Several methodologies can be employed for its quantification. Some of the most common approaches include setting vehicle dynamics response thresholds (Parsons and Griffin, 1988; Sohn et al., 2019). These thresholds are determined on the basis of self-reported scores (Smyth et al., 2018; Zhu et al., 2022) or by monitoring physiological signals (Aledhari et al., 2023), such as heart rate variability (HRV), systolic blood pressure (SBP), and galvanic skin response (GSR). Although vehicle dynamics response thresholds cannot accurately reflect all occupants' feelings due to subjective differences, reasonable threshold quantities and values can be correlated to the subjective preference of the majority of individuals and effectively employed to guide vehicle design and control (Hayafune and Yoshida, 1990). Thus, vehicle dynamics response thresholds are widely used and many standards specify dynamics thresholds to guide the design of vehicles.

Referring to vehicle longitudinal motion, comfort is often related to the smoothness of acceleration and deceleration, which is described by jerk, i.e. longitudinal acceleration derivative (Huang and Wang (2004)). In particular, the maximum absolute value of jerk is commonly used as a metric to evaluate driving style and comfort. In the literature, different thresholds related to maximum jerk can be found. Hoberock (1976) and Hubbard and Youcef-Toumi (1997) recommend, for passenger cars, not to exceed a maximum jerk of 0.3 g/s (2.94 m/s^3) to ensure passengers' comfort. In case of public transportation vehicles, the maximum jerk that an occupant can withstand without losing balance is approximately 0.60 m/s^3 (Martin and Litwhiler, 2008). Bae et al. (2019) pointed out that the jerk threshold for ride comfort is approximately between 0.3 and 0.9 m/s^3, and can be reasonably set to 0.9 m/s^3 (Bae et al., 2020). Additionally, the ISO standard (ISO 15622:2018(E), 2018) outlines that the maximum negative longitudinal jerk should not exceed 2.5 m/s^3 at speed above 20 m/s and 5 m/s^3 at speed below 5 m/s for adaptive cruise control.

However, driving comfort and energy saving are in conflict with each other (Sohn et al., 2020). Considering the interaction between ride comfort and energy saving, several papers consider both jerk and fuel consumption minimization while optimizing eco-driving strategies (Nandi et al., 2015; Wu et al., 2019; Chada et al., 2023). For the PnG strategy, rapid transitions between acceleration and deceleration are typically required to achieve highly efficient operation of the powertrain system, which would generate a large jerk and, consequently, cause discomfort. Sohn et al. linked ride comfort to the jerk value of the PnG strategy by subjective evaluation while riding in a real vehicle (Sohn et al., 2019). Results show that the absolute jerk value of the comfort level defined as 'noticeable only to skeptical customers' should be below 0.4 m/s^3 and 0.6 m/s^3 during the acceleration to deceleration transition phases. Furthermore, based on this investigation, an analysis of the tradeoff between fuel economy and ride comfort for a 1.2-liter engine has been conducted (Sohn et al., 2020), showing that an additional energy saving up to 5% can be achieved when ride comfort is not considered. A similar work was conducted for a battery electric vehicle (BEV) with a high efficient motor (Xue et al., 2024). The result shows that the optimal PnG strategy is able to save up to 5% energy compared with the corresponding CS strategy, and a reduction of about 1% energy saving can be found when a constraint of maximum jerk is considered.

Physical prototypes are typically needed to validate the driving strategy and evaluate ride comfort. With the development of driving simulation technologies, able to realistically simulate various driving scenarios, there is the potential of performing such evaluations in a safe, efficient, and realistic environment without needing physical prototypes.

Driving simulators have been widely used for analyzing the driver response to ADAS and AVs (Gouribhatla and Pulugurtha, 2022; Orlovska et al., 2020; Aramrattana et al., 2021; Steimle et al., 2025). The potential effects of ADAS on driver behaviors across different driving scenarios, lighting conditions, and weather conditions was analyzed by using driving simulator (Orlovska et al., 2020). With reference to eco-driving strategy validation, Stabile et al. (2023) successfully used a nine-degree-of-freedom dynamic driving simulator to study the impact of driver behavior and traffic conditions on the ecological driving strategy of an urban concept light electric four-wheel vehicle. In Chada et al. (2023), the validation of a predictive eco-driving assistance system (pEDAS), designed to assist drivers in optimizing their behaviors to minimize energy consumption in BEVs, has been validated by using a dynamic driving simulator. The result shows that pEDAS exhibits promising potential, not only in reducing overall energy consumption, but also in promoting driver compliance with speed limits and avoiding unnecessary stops at signalized intersections.

Referring to comfort evaluation, several application of driving simulators can be found in the literature (for a literature review see Xue et al., 2023 and Bruck et al., 2020). Dynamic driving simulators can exhibit a good correlation between vehicle dynamic performance with driver behavior and subjective perceptions (Sekar et al., 2022). In Arconada et al. (2023), a dynamic simulator based on a Stewart platform was employed to perform ride comfort tests in the 1–10 Hz frequency range, demonstrating that the driving simulator has a strong capability of whole-body vibration comfort evaluation in this frequency range. In de Winkel et al. (2023), the impact of transient motion on ride comfort was investigated using a driving simulator. The study considered simple acceleration and jerk profiles to provide a parametrization of expected discomfort for AVs. The comfort in high-level AV driving styles are investigated by using a motion-based driving simulator in Peng et al. (2025). Interestingly, in contrast to the general idea of minimizing jerk magnitude, both de Winkel et al. (2023) and Peng et al. (2025) reached to a similar conclusion that a higher jerk, usually with a shorter duration, may result in a more comfortable driving experience, and highlighted that the duration of jerk needs to be taken into account when evaluating the longitudinal comfort. In Xue et al. (2024), the optimal PnG strategies with and without comfort considerations were subjectively evaluated using a dynamic driving simulator, and the results highlighted a strong correlation between objective jerk data and human subjective perceptions, demonstrating the rationality of the selected jerk threshold (0.9 m/s^3) and the potential of driving simulators in evaluating longitudinal comfort.

Compared with real vehicles, driving simulators have a capability of controling vehicle accurately and safely and can effectively simulate the comfort level under different driving conditions, thus providing reliable data support for the setting of comfort evaluation. However, existing studies seldomly explore the correlation of the longitudinal comfort between driving simulators and real vehicles to further demonstrate the potential of driving simulators in comfort evaluation of eco-driving strategies.

With the aim to investigate the ride comfort of the PnG strategy by using a dynamic driving simulator, the paper first presents a comprehensive approach to estimating the longitudinal comfort thresholds in

Table 1
Parameters of the electric vehicle.

	Value
Curb mass + driver	1700 kg
Drag coefficient	0.32
Frontal area	2.3 m^2
Air density	1.225 kg/m^3
Tyre model	215/50 R17
Tyre resistance coefficient	0.013
Suspension (F/R)	MacPherson/Multi-link
Height	1594 mm
Width	1765 mm
Length	4166 mm
Track (F/R)	1501/1501 mm
Wheelbase	2601 mm
Peak Torque	360 Nm
Peak Power	150 kW
Peak Power density	28.8 W/cm^2
Max speed	8810 rpm
Number of poles	8
Differential drive ratio	7.05
Differential efficiency	0.902

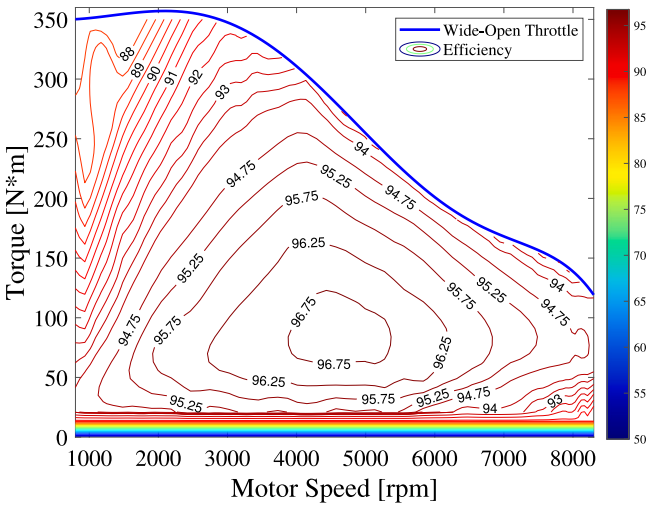

Fig. 1. Efficiency map of motor. *Source:* Adapted from Momen et al. (2016).

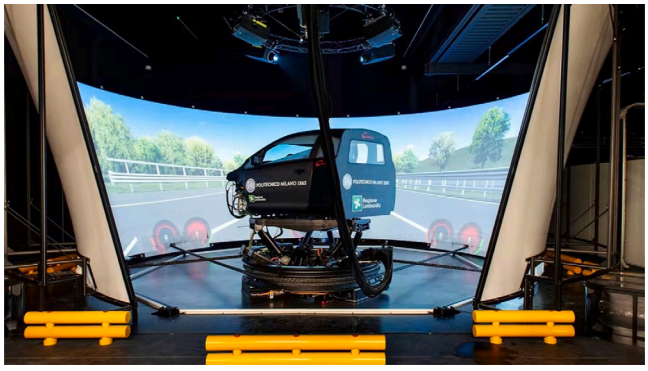

Fig. 2. 9-DOF cable-driven dynamic driving simulator at DriSMi (DriSMi, 2025).

an eco-driving strategy using a driving simulator to validates the correlation with the real car. Furthermore, the obtained thresholds, which represents drivers' comfort preferences, are used to define and validate a procedure for PnG optimization to balance energy consumption and ride comfort.

The paper is organized as follows. Firstly, Section 2 introduces the vehicle model used throughout the paper. The model is exploited both for the experimental tests with the dynamic driving simulator and as reference model for the PnG strategy optimization. The dynamic driving simulator is described in 3. Particular attention is devoted to the definition of the driving simulator feedback behavior, i.e. the so called cueing algorithm. The experimental procedure for the estimation of jerk thresholds is described in Section 4 along with the experimental results. The identified thresholds are exploited in Section 5 for the optimization of the PnG strategy. In this section, the optimization procedure, comprising the definition of the optimization problem, the multi-objective solution, and the optimized strategies, is presented. Finally, Section 6 is devoted to the experimental verification of the obtained optimal strategies. Section 7 concludes the paper.

2. Mathematical model of the vehicle

In this section, the mathematical model of the reference vehicle is described. The considered vehicle is a Bolt EV. This vehicle is an electric sedan car whose data has been obtained from open access repository (www.evspecifications.com, 2020) and summarized in Table 1. In particular, motor efficiency data has been taken from Momen et al. (2016) and adapted to obtain the map of Fig. 1.

The vehicle dynamic model developed in Xue et al. (2024) is employed. The vehicle model has been realized by using the commercial software VI-CarRealTime by VI-Grade (VI-grade GmbH, 2021). The resulting model is a 14-degree-of-freedom vehicle model, including subsystems such as body, braking, suspension, tires, steering, and powertrain systems. In particular, the motor efficiency map has been integrated into the powertrain system. Due to a lack of data and to simplify the powertrain model, an ideal zero-torque coasting is assumed. The inertia properties of the vehicle have been estimated based on the mass and dimensional parameters of the vehicle according to Gobbi et al. (2014). Finally, due to the short duration of the maneuver, a fixed state of charge (SOC) and constant voltage of the battery are assumed.

The vehicle model, in particular longitudinal dynamic performance and energy consumption, has been validated by the public-available data of the reference vehicle (www.evspecifications.com, 2020). The comparison of the acceleration time, top speed, braking distance, and energy consumption (combined city and highway EPA driving test) of the vehicle model with respect to reference data are shown in Table 2.

As shown in Table 2, the model is able to well approximate the longitudinal dynamics and energy consumption, with errors of less than 3% for maximum speed, less than 1% for braking distance, and 1.2% for the combined EPA test. The model slightly overestimates the acceleration time (with a maximum variance of about 8%), which may be caused by differences related to the actual configuration of the test vehicle, such as effective mass and grip conditions.

3. Dynamic driving simulator

The cable-driven 9-DoF VI-grade DIM400 dynamic driving simulator of the DriSMi laboratory (DriSMi, 2025) of Politecnico di Milano (shown in Fig. 2) is employed to conduct the tests. The driving simulator features two actuation stages for the simulation of the vehicle motion. The first stage consists of a cable-driven platform able to move in the plane and rotate around the vertical axis. This stage can reproduce low frequency motions up to 3 Hz. The second stage is a modified Steward platform with 6 degrees of freedom able to reproduce higher frequencies motions up to 30 Hz. Furthermore, eight on-board shakers are connected to the cockpit at the suspension points for higher frequency vibrations up to 200 Hz. Table 3 summarizes the motion-related specification of the DIM400 driving simulator.

Table 2
Vehicle model validation. Comparison between numerical simulations and vehicle reference data available at www.evspecifications.com (2020).

	Vehicle model	Ref. (www.evspecifications.com, 2020)	Relative error
5–60 mile/h	7.23 s	6.70 s	7.3%
30–50 mile/h	2.67 s	2.50 s	6.3%
50–70 mile/h	4.05 s	3.70 s	8.6%
70–0 mile/h	57.93 m	58.22 m	0.5%
top speed	149.3 km/h	145 km/h	2.9%
EPA combined	119.5 MPGe	118 MPGe	1.2%

Table 3
Motion-related specifications of DIM400 at DriSMi.

	Value
Longitudinal/lateral displacement range [m]	±2
Vertical displacement range [m]	±0.298
Pitch/roll displacement range [deg]	±15
Yaw motion range [deg]	±62
Maximum longitudinal/lateral acceleration [g]	1.5
Maximum vertical acceleration [g]	2.5
Maximum longitudinal jerk [m/s^3]	2 e + 05

Due to the limited workspace, driving simulators cannot fully reproduce the motion of the real car, but a motion cueing algorithm has to be introduced to convert the vehicle dynamic response into a feasible driving simulator motion range (Fisher et al., 2011). Thus, a model predictive control (MPC)-based algorithm is employed to provide motion perceptions to the driver (VI-grade GmbH, 2022; Bruschetta et al., 2017). To provide a more realistic and immersive experience, the simulator is equipped with active seat cushions and active seat belts to enhance the driver's perception of longitudinal acceleration. A 270° wrap-around screen and a system of five speakers provide the visual and auditory feedback to the driver (more details in Melzi and Previati, 2024).

4. Subjective ride comfort evaluation by using the dynamic driving simulator

In this section, the experimental activities completed at the dynamic driving simulator for the evaluation of the perceived longitudinal ride comfort are described. In particular, the tests aim to the identification of different jerk thresholds related to different comfort perceptions of the occupants.

4.1. Jerk thresholds definition

The objective of the tests is to identify three different jerk levels related to different perceptions of the testers. The investigated thresholds are defined as follows.

- Threshold 1: noticeable jerk. Testers find the vehicle comfortable but notice a difference with respect to constant velocity.
- Threshold 2: annoying jerk. Testers find the vehicle no more comfortable and they feel annoyed by the continuously changing acceleration.
- Threshold 3: unbearable jerk. Above this jerk value, the vehicle is too uncomfortable and the corresponding strategy should be considered as a failure.

In Sohn et al. (2019), it is pointed out that ride comfort is not only related to maximum jerk but also to maximum longitudinal acceleration. In traditional internal combustion engine vehicles, this relationship is particularly critical. In fact, according to Xu et al. (2015), the optimal PnG strategy always makes the powertrain system of internal combustion engine vehicles operating in regions close to the maximum available torque. In this case, therefore, high longitudinal accelerations can be expected. In this paper, we consider electric vehicles whose motors exhibit large high-efficiency areas, also at relatively low levels of torque (see Fig. 1). High longitudinal accelerations are not required for these vehicles and jerk plays the most important role. For these reasons, in the following tests and optimization, only the jerk value is considered.

In the following subsections, the driving simulator settings, the test procedure, and the collected results are described.

4.2. Dynamic driving simulator set up

Drivers on autonomous cars are like passengers and most of the time they do not need to interact with the steering wheel or the pedals. To realistically reproduce this scenario on the driving simulator, pedals and steering wheel are disabled and the vehicle is controlled by a control algorithm. This control implements a simple Kondo's shaft driver model (Plöchl and Edelmann, 2007) for controlling the steering angle and keeping the straight line trajectory, while the accelerator is controlled to obtain the desired jerk values.

The PnG-like strategy is centered around a reference velocity v_0 as depicted in Fig. 3. Starting from v_0, the vehicle is accelerated up to a higher velocity level v_u. When v_u is reached, the accelerator is released, and the vehicle decelerates to a lower velocity level v_l. Once v_l is reached, the accelerator is opened, and the velocity increases, resuming the cycle. Different reference velocities v_0 are considered in the tests, namely 50 km/h, 80 km/h, and 130 km/h.

As depicted in Fig. 3, for the reference velocity v_0 different PnG-like strategies are considered, resulting in different velocity cycles. These strategies differ only in the time required for opening or closing the accelerator. In fact, the maximum jerk reached in each cycle is determined only by the way in which the accelerator command is varied. Clearly, slower accelerator releases result in higher maximum velocities reached during the cycle. These (small) differences in the maximum velocities are not relevant as they are not perceivable by the testers and the actual mean velocity in the cycle is not the subject of this study. Finally, during the acceleration phase, the accelerator amplitude is kept constant and selected to maintain the motor in the high-efficiency area for each reference velocity. The accelerator command is set to 20%, 25%, and 50% for 50 km/h, 80 km/h, and 130 km/h, respectively.

The fidelity of driving scenario influences driver responses (Mussone, 2023). Therefore, a 3-line highway scenario without any traffic interaction, featuring detailed road geometries and signals, and realistic visual textures closely resembling a real-world driving environment (as shown in Fig. 4) has been developed and integrated into the driving simulator.

Motion cueing plays a vital role in improving realism and the driver's perception of vehicle velocity and road conditions (El hamdani et al., 2023; Zhao et al., 2024). In El hamdani et al. (2023) the effects of motion cueing on drivers' braking behavior are investigated. Three different levels of motion cueing (no motion, moderate motion, and maximal possible response and range) are created for the evaluation. Results show that the higher level of motion cueing, i.e., maximal response and range, would yield a close correlation with real car data, enhancing drivers' vehicle control and vehicle velocity perception. In addition, motion cueing has been proven to be correlated to road

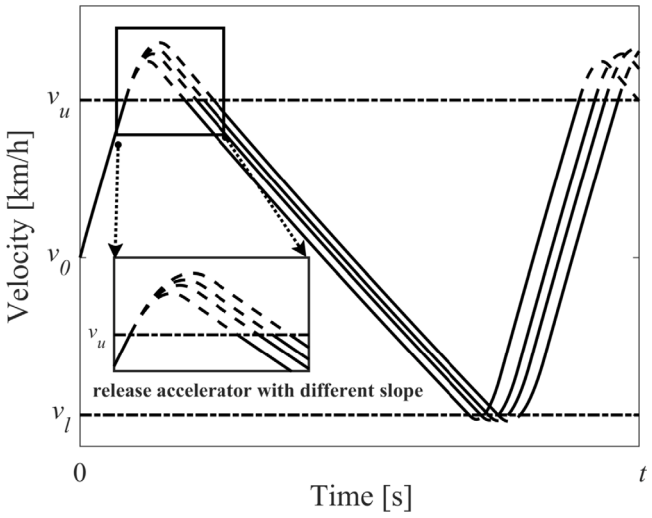

Fig. 3. Velocity profile generated by the PnG-like control strategy.

Fig. 4. 3-line highway scenario without any traffic interaction.

surface sensing of drivers (Zhao et al., 2024). Therefore, to provide a realistic driving experience, the motion cueing parameters of the simulator have been optimized to reproduce the maximal possible dynamic response and motion range.

Fig. 5(a) displays the jerk signal that has been considered. The reference jerk is the one derived from vehicle model and the actual jerk perceived by passengers is the one defined by motion cueing. The initialization phase of the maneuver has been removed in Fig. 5(a). Fig. 5(b) depicts the corresponding power spectral densities (PSD) of the signal in Fig. 5(a). The optimized motion cueing algorithm can accurately reproduce the jerk response of the vehicle model, with only minor differences in the positive jerk peak value. Considering the PSD comparison, the utilized motion cueing reproduces the response up to about 25 Hz, close to the simulator's maximum frequency of 30 Hz. Also, the response above 25 Hz is attenuated to approximately −60 dB/Hz, giving a small contribution to the perceived motion. To complete the motion feedback, active cushions are utilized to provide the feeling of constant longitudinal acceleration. Finally, to avoid influencing participants' perceptions, the dashboard of the vehicle is turned off.

4.3. Test procedure

The estimation of the three thresholds defined in Section 4.1 has been performed according to the up-down method (Levitt, 1971). This method finds out the perception threshold by an iterative approach. Each participant is subjected to different stimulus levels. Each level is adjusted on the basis of the participant's response to the previous level. In particular, the stimulus is increased of a predefined amount if it is not felt by the participant or reduced otherwise. The test is ended when the increase/decrease direction is inverted at least four times. The identified threshold is then computed as the mean value of the jerk values before and after the last two increase/decrease inversions. The up-down method has been proven to be efficient for the estimation of the perception threshold requiring a reduced total number of tests compared to conventional self-reported scoring methods (Levitt, 1971; Soranzo and Grassi, 2014).

Table 4
Questions asked to each participant for each jerk threshold and initial jerk levels. Jerk thresholds defined in Section 4.1.

Threshold n°	Question to the participant	Initial jerk level
1	Can you notice the jerk during traveling?	0.4 m/s^3
2	Do you feel annoyed by the jerk during traveling?	0.9 m/s^3
3	Do you think this driving strategy is too uncomfortable to accept?	2.5 m/s^3

Algorithm 1 introduces the process of the subjective experiment using the up-down method. Tests are organized as follows. Each participant repeats the test for the three considered velocities, 50 km/h, 80 km/h, and 130 km/h. For each velocity, the up-down approach is applied for the identification of the three thresholds defined in Section 4.1. The questions used for the identification of each threshold are reported in Table 4. In the same table, the initial jerk value for each threshold is reported. The same questions and initial jerk values are used for all of the considered velocities. For all tests, the same step size of 0.1 m/s^3 is used. Each participant performs a total of nine up-down procedures to identify the three thresholds for each of the three considered velocities. At the beginning of each test, the participant is informed of the reference velocity level and of the type of threshold.

Algorithm 1: Comfort threshold estimation using up-down method

Input: Participant's answer: Yes/ No;
Step size: Δ_s;
Output: Estimated threshold *Threshold*
while $N_{rev} < 4$ **do**
  evaluate the current jerk level $\text{Jerk}^{(j)}$, and give the answer;
  if $answer^{(j)} \neq answer^{(j-1)}$ **then**
    $T^{(N_{rev})} = (\text{Jerk}^{(j-1)} + \text{Jerk}^{(j)})/2$ $N_{\text{rev}} = N_{\text{rev}} + 1$
  if $answer^{(j)} =$ *"Yes"* **then**
    $\text{Jerk}^{(j+1)} = \text{Jerk}^{(j)} - \Delta_s$
  else
    $\text{Jerk}^{(j+1)} = \text{Jerk}^{(j)} + \Delta_s$
  $j = j + 1$
Threshold $= (T^{(N_{\text{rev}}-1)} + T^{(N_{\text{rev}})})/2$
return *Threshold*;

The initial jerk values reported in Table 4 have been chosen from similar conditions considered in previous papers from the literature. In particular, for threshold 1, the initial jerk corresponds to the jerk threshold identified in Sohn et al. (2019) for the jerk level defined "noticeable for all customers". For threshold 2, the initial jerk level corresponds to the level of aggressive driving defined in Bae et al. (2020), while threshold 3 corresponds to the limitation on the maximum jerk for ACC defined in ISO standard (ISO 15622:2018(E), 2018).

In case of very low values of jerk, a slight modification of the method has been introduced due to the motion range of the dynamic driving simulator. Specifically, by using the optimized cueing settings discussed in Section 4.2, the longitudinal displacement of the driving simulator limits the minimum reproducible jerk value to 0.2 m/s^3. Below this jerk value, the displacement limits are reached and the test cannot be performed. Therefore, in the identification of Threshold 1, if

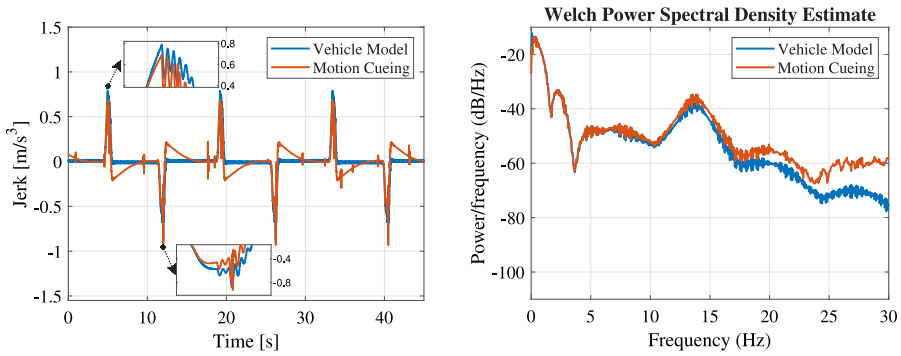

(a) Time history (b) Frequency domain

Fig. 5. Comparison between the jerk output of optimized motion cueing and the jerk simulated by the vehicle model.

Table 5
Estimated thresholds of jerk for different comfort levels.

	50 km/h			80 km/h			130 km/h		
Threshold	1	2	3	1	2	3	1	2	3
Participant 1	0.65	1.1	2.4	0.55	1.1	2.7	0.45	0.85	2.2
Participant 2	0.25	0.75	1.7	0.25	0.7	1.8	0.35	0.65	1.7
Participant 3	0.5	0.85	2.4	0.45	0.95	2.25	0.65	0.95	2.4
Participant 4	0.5	1.05	2.3	0.35	0.75	2.1	0.35	0.95	1.7
Participant 5	0.2	0.65	2.4	0.35	0.85	1.8	0.35	0.7	2.1
Participant 6	0.35	0.65	1.7	0.25	0.65	1.7	0.3	0.5	1.7
Participant 7	0.3	0.85	2.3	0.35	0.9	2.25	0.3	0.95	2.25
Participant 8	0.2	0.75	2.1	0.2	0.95	1.7	0.25	0.9	2.4
Ref	0.4	0.9	2.5	0.4	0.9	2.5	0.4	0.9	2.5
Mean	0.37	0.83	2.16	0.34	0.86	2.04	0.38	0.81	2.06
Std	0.16	0.17	0.30	0.11	0.15	0.35	0.13	0.17	0.31
95% CI	[0.23, 0.51]	[0.69, 0.97]	[1.91, 2.41]	[0.25, 0.44]	[0.73, 0.98]	[1.74, 2.33]	[0.27, 0.48]	[0.66, 0.94]	[1.79, 2.32]

the current level is 0.2 m/s^3 and the participant identifies this level as noticeable, instead of reducing the jerk value, the initial guess of 0.4 m/s^3 is restored. From this value, the sequence is resumed. If, again, the participant reaches 0.2 m/s^3 and identifies this value as noticeable, the test is interrupted. In this case, the participant is interviewed to understand if he or she considers that this level could be the threshold or expects to notice a lower value of jerk. In the performed tests, only 2 participants found themselves in this situation, and they all believed that this level of jerk was the least they would be able to experience. Therefore, for those participants, 0.2 m/s^3 is considered as the identified threshold.

4.4. Estimated thresholds

For the experimental identification of the jerk thresholds, eight participants have been recruited (drivers' information in Table A.11). The number of participants is relatively low, but comparable with similar experiments reported in the literature (Sohn et al., 2019). The limited number of participants allows for a preliminary analysis and the obtained results should be further investigated with a larger panel of participants. However, to the best knowledge of the authors, similar tests with dynamic driving simulators are not available in the literature and these tests provide a first, even if preliminary, assessment of the perceived longitudinal comfort on a driving simulator. All of the participants possess a driving license and a total of 366 trials were conducted for the estimation of the thresholds. Table 5 and Fig. 6 show the estimated thresholds for different comfort levels at the three considered reference velocities. In particular, the statistical metrics, such as mean value, standard deviation (std), and 95% confidence interval (95% CI), have been calculated, and shown in Table 5.

Results show a rather good agreement between the thresholds identified at the driving simulator and previously published data referring

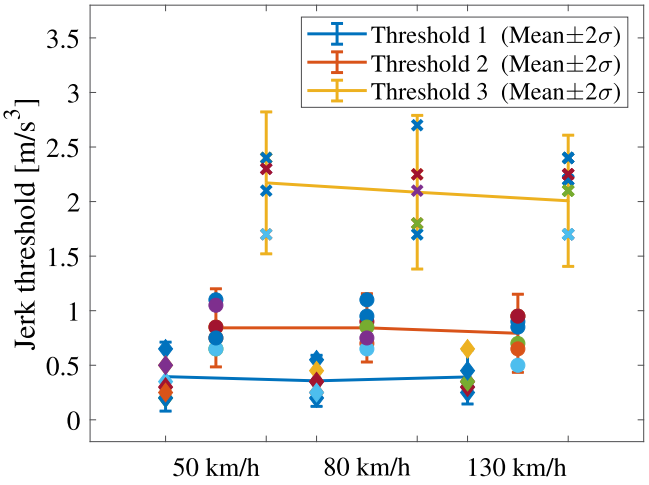

Fig. 6. Estimated thresholds of jerk for different comfort levels — different colors of scatters represent different participants.

to tests performed on real cars. In particular, the mean value of the estimated Threshold 1 and Threshold 2 closely match the reference values of 0.4 m/s^3 and 0.9 m/s^3, respectively. Additionally, for all reference speeds, the reference values of both Threshold 1 and Threshold 2 reported in the literature fell within the 95% confidence intervals of the thresholds estimated using the driving simulator. Additionally, the estimated range of Threshold 1 is from 0.2 m/s^3 to 0.65 m/s^3, and closely matches the results of the subjective experiments in Sohn et al. (2019). Threshold 3 shows an identified level of jerk moderately lower than the value of 2.5 m/s^3 suggested as limit by the standards (ISO

15622:2018(E), 2018). Moreover, as shown in Table 5, the estimated Threshold 3 values for most participants are lower than the value reported in the literature. This can be attributed to the test configuration, in which the PnG strategy repeatedly generates jerk peaks, leading to greater perceived discomfort compared to the emergency braking defined in the ISO standard (ISO 15622:2018(E), 2018), where jerk is applied only once. Also, the estimated value of jerk for this threshold shows a relatively large variation with subjective estimations ranging between 1.7 m/s^3, and 2.7 m/s^3. Finally, from the inspection of Fig. 6, estimated jerk thresholds seem to be independent from the reference velocity.

5. Multi-objective optimization

The values of the thresholds on jerk perception estimated in the previous section are exploited for the optimization of the PnG strategy of the considered electric vehicle. The Pareto optimal set is able to provide the best trade-off between energy consumption and ride comfort. The offline Pareto optimal solution under different working conditions (average velocity) would be helpful as a reference input into the vehicle control system, allowing the control system to select the optimal strategy on the Pareto optimal set as the real-time control strategy according to demand. In particular, different Pareto points with different levels of jerk can be dynamically selected based on real-time traffic conditions or driver preference of energy consumption and ride comfort to achieve adaptive control. Therefore, the optimization is performed by a multi-stage approach comprising the following steps.

- Definition of the optimization problem in a multi-objective framework (Pareto optimization).
- Computation of an initial Pareto-optimal set by means of a neural network surrogate model trained by simulating the vehicle model described in Section 2.
- Refinement of the obtained Pareto-optimal set by directly using the physical model described in Section 2.
- Validation of the obtained Pareto-optimal set by experimental tests at the dynamic driving simulator

In the following sections, these steps are discussed.

5.1. Design variables

The smoothed accelerator pulse width modulation (PWM) command is periodically repeated to control the vehicle velocity. The command is parameterized as shown in Fig. 7. Six design variables, namely five time durations t_i, $i = 1...5$ of the different command intervals and accelerator amplitude A are used to define the shape of the accelerator command signal as

$$\begin{aligned} y(t) &= y_{rise}(t) + y_{fall}(t),\ 0 \le t \le t_{cycle} \\ y_{rise}(t) &= \frac{A}{t_2}\log\left(\frac{1+e^{\beta\cdot(t-t_1)}}{1+e^{\beta\cdot(t-t_1-t_2)}}\right)^{\frac{1}{\beta}} \\ y_{fall}(t) &= \frac{A}{t_4}\log\left(\frac{1+e^{\beta\cdot(t-t_1-t_2-t_3)}}{1+e^{\beta\cdot(t-t_1-t_2-t_3-t_4)}}\right)^{\frac{1}{\beta}} \end{aligned} \tag{1}$$

where the parameter β ($\beta > 0$) is introduced to control the curvature of the transition zone (Dombi and Gera, 2005) and is fixed to 20. It is important to highlight that the optimization is performed based on the offline simulation, in which a total of 8 driving cycles are conducted: the first 4 cycles are used to stabilize the vehicle speed, while the last 4 cycles are used to calculate the vehicle response. t_5 is treated as a redundant design variable, which expands the optimization space and enhances flexibility in controlling the vehicle, to ensure that the vehicle stabilizes as quickly as possible during offline optimization. The design variables and related ranges are summarized in Table 6.

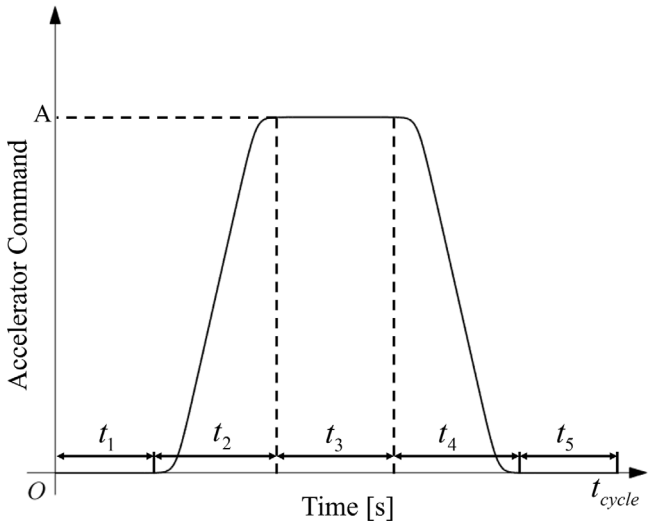

Fig. 7. Smoothed accelerator command and design variables.

Table 6
Design variables of the optimization problem (t_i in seconds).

Description	Notation	Range
Starting interval	t_1	[0.001, 10]
Rising interval	t_2	[0.001, 10]
Plateau interval	t_3	[0.001, 10]
Falling interval	t_4	[0.001, 10]
Ending interval	t_5	[0.001, 10]
Magnitude	A	[0, 1]

5.2. Optimization problem definition

In the PnG strategy, energy consumption and ride comfort usually conflict with each other (Sohn et al., 2020). Thus, a two-objective functions minimization problem is defined as follows

$$\begin{aligned} &\min_{\boldsymbol{x}}\ \boldsymbol{f}(\boldsymbol{x}) = \left\{E_{\mathrm{PnG}}(\boldsymbol{x}),\ J(\boldsymbol{x})\right\} \\ &\text{s.t. } \left|v_{\mathrm{A}}(\boldsymbol{x}) - v_{\mathrm{T}}\right| \le 0.1 \\ &\quad \boldsymbol{x} \in \boldsymbol{X} \end{aligned} \tag{2}$$

where $\boldsymbol{x}$ is the vector of the design variables, namely $t_1, \ldots, t_5$, and A, $\boldsymbol{f}(\boldsymbol{x})$ is the vector of the objective functions, $E_{\mathrm{PnG}}(\boldsymbol{x})$ the energy consumption per traveling distance (kWh/m), $J(\boldsymbol{x})$, the maximum absolute value of the jerk (m/s^3), see Eq. (3), v_{A} the average vehicle velocity (km/h), see Eq. (4), v_{T} the reference velocity (km/h), and $\boldsymbol{X}$ the feasible design variable domain.

$$E_{\mathrm{PnG}}(\boldsymbol{x}) = \frac{E_{4cycle}(\boldsymbol{x})}{\Delta x} \tag{3}$$

where, both $E_{4cycle}(\boldsymbol{x})$ and Δx are calculated by VI-CarRealTime software. $E_{4cycle}(\boldsymbol{x})$ is the total energy consumption (kWh) in the last four cycles of the eight. Δx is the travel distance (m) in the last four cycles.

$$J(\boldsymbol{x}) = max\left|\frac{\Delta a_x(\boldsymbol{x})}{\Delta t}\right| \tag{4}$$

where, $\Delta a_x(\boldsymbol{x})$ is the longitudinal acceleration changed in each time step derived from Vi-CarRealTime, and Δt is the time step of the simulation result output, 0.01s.

The optimization problem is solved according to the Pareto optimal theory (Papalambros and Wilde, 2000), which consists in finding the set of solutions representing the best compromise between $E_{\mathrm{PnG}}(\boldsymbol{x})$ and $J(\boldsymbol{x})$, while fulfilling the constraints.

5.3. Optimization procedure

Although the optimization problem stated in Eq. (2) includes only two objective functions, the constraint on the mean velocity is rather binding as a large number of simulations are required to find a feasible solution. By using the physical model of Section 2, each simulation takes from a few seconds to 5 min on a laptop with AMD Ryzen 7 5800H 3.20 GHz and 16 GB of RAM and the whole process would require a non-feasible amount of time. Therefore, a surrogate model and a two-stage solution procedure have been developed to reduce the computational time. The first stage exploits the surrogate model to quickly obtain a preliminary Pareto optimal set. On the basis of the solutions obtained in the first stage, in the second step, the physical model is employed to obtain the final optimal solutions. Fig. 8 shows the main structure of the optimization framework.

The surrogate model to approximate the vehicle response in the first stage is a neural network (NN) with one hidden layer of 20 neurons, and a tangent sigmoid activation function. The NN is trained by using a dataset of 3500 initial samples generated in the feasible domain by a low-discrepancy Sobol sequence (Mastinu et al., 2007). Of these samples, 70% are randomly sampled for training and the remainder 30% for validation. The NN receives as input the parameters describing the accelerator profile and outputs the energy consumption, average velocity, and maximum jerk. Mean squared error (MSE) and R-square (R^2) are used for monitoring the fitting performance of the trained NN. To ensure optimal model performance and robustness, a systematic hyperparameter optimization was conducted based on a DOE test. The DOE considers three levels for the learning rate, namely [0.001, 0.01, 0.05] and three different training algorithms, namely ["traincgf" (Fletchel-Powel Conjugate), "trainlm" (Levenberg–Marquardt), "trainscg" (Scaled Conjugate Gradient)]. This resulted in 9 different combinations of parameters. Each configuration was evaluated based on its performance in the validation set, with the optimal combination selected according to the minimum MSE criterion. The best result was obtained with a learning rate of 0.01 combined with the Levenberg–Marquardt training algorithm. To avoid overfitting, L2 regularization with a coefficient of 0.001 was applied, penalizing large weight values and promoting simpler models. Furthermore, the training and validation loss curves were monitored throughout the learning process. The trained NN is exploited by a genetic algorithm (GA) for the computation of the approximated Pareto optimal set. The GA features a population size of 200 individuals and a maximum of 200 generations is considered. The solutions of the approximated Pareto-optimal set are then recomputed by using the physical model in order to verify the accuracy level of the NN for solutions close to the actual Pareto-optimal set. If the relative error between the objective functions computed by the NN and the physical model is above 2%, the NN is retrained by adding the solutions in the dataset and the procedure is iterated. In particular, the updated dataset is randomly sampled as in the previous iteration, with the condition that the newly generated data is included in the training set. The same neural network structure and training parameters are used for all iterations. When the relative error E is below 2% the first stage of the optimization is concluded. The relative error between NN Pareto optimal set $\hat{\boldsymbol{f}}(\hat{\boldsymbol{x}})$ and the corresponding output of the physical model $\boldsymbol{f}(\hat{\boldsymbol{x}})$ is defined as

$$E = max\{\bar{E}_1, \bar{E}_2, \bar{E}_3\} \tag{5}$$

where, $\bar{E}_1, \bar{E}_2, \bar{E}_3$ are the average relative error in terms of the energy consumption, maximum jerk, and average velocity, respectively, which are defined as

$$\bar{E}_j = \frac{1}{n}\sum_{i=1}^{n}\frac{\left|f_j(x_i) - \hat{f}_j(x_i)\right|}{\left|f_j(x_i)\right|},\ j = 1,2,3 \tag{6}$$

where, n represents the Pareto size, f_j, and $\hat{f}_j$ are the output of the physical model and of the NN, respectively.

In the second stage, the approximated Pareto optimal set obtained is refined, and the physical model is exploited in place of the NN for the computation of the objective functions and constraints. Considering the increased computational effort with the use of the physical model, the population size is reduced to 100 individuals at this stage. All the 200 Pareto-optimal points obtained from the first stage are simulated by the physical model and the relative fitness function is computed again for each individual. The newly computed fitness values may differ from the previous ones because of the small approximation errors of the NN model. These individuals are then ranked according to their fitness value and the best 100 points are selected as the starting population for the second-stage of the optimization. In this selection process the following two situations can happen

- the number of optimal points is less than 100: in this case also non-optimal points are randomly included in the population
- the number of optimal points to be included is more than 100: in this case 100 points are randomly selected from the optimal ones.

It has to be emphasized that the described selection procedure is only affecting the way of building the starting population of the refined optimization process and has a negligible effect on the convergence rate of the algorithm.

In the two stages of the optimization procedure, the same multi-objective GA algorithm (Gobbi, 2013) is employed to solve the optimization problem. The difference between the two stages is that the objective functions are computed in the first stage by the surrogate model, while in the second stage are computed by the physical model. The multi-objective GA algorithm is based on the fitness sharing method (Mastinu et al., 2007). The fitness F_i of each individual i is defined as follows

$$F_i = \frac{N_r - rank(i) + 1}{\sum_{rank=1}^{N_r}\left(N_r - rank(i) + 1\right)\cdot P_{si}/P} \tag{7}$$

where, $rank(i)$ and P_{si} are the dominance rank of individual i and the population of $rank(i)$, respectively. N_r is maximum rank in the current generation, P is the population size. The non-dominated points in the whole population are assigned rank 1. Among the remainder population, non-dominated individuals are ranked 2. The ranking procedure continues until the whole population is involved.

In order to avoid individuals moving into crowded areas and to obtain a uniformly distributed Pareto optimal set, the fitness function is modified by a fitness sharing method (Mastinu et al., 2007). The fitness function $\overline{F_i}$, to be maximized, for each individual i with fitness F_i is defined as

$$\overline{F_i} = F_i - \alpha_1 m_i - \alpha_2 \Delta_i \tag{8}$$

where, the coefficients α_1 and α_2 are the scaling factors of the niche count m_i. A penalty term Δ_i in included to avoid constraints violation.

The niche count m_i measures the approximate number of individuals sharing fitness (Sareni and Krahenbuhl, 1998), and is described by Eq. (9)

$$m_i = \sum_{j=1}^{P}\mathrm{sh}\left(d_{ij}\right) \tag{9}$$

where, d_{ij} is the distance between individuals i and j, and the sharing function $\mathrm{sh}\left(d_{ij}\right)$ is defined as follow

$$\mathrm{sh}\left(d_{ij}\right) = \begin{cases} 1 - \left(d_{ij}/\sigma_s\right)^2 & ,\ \text{if } d_{ij} < \sigma_s \\ 0 & ,\ \text{otherwise} \end{cases} \tag{10}$$

where, σ_s stands for the threshold of dissimilarity, i.e., the niche radius (Sareni and Krahenbuhl, 1998).

The penalty term Δ_i of each individual i accounts for the violation of the velocity constraints and is defined as

$$\Delta_i = \begin{cases} (v_A^{(i)} - v_T)^2 & ,\ |\ v_A^{(i)} - v_T\ | > 0.1 \\ 0 & ,\ \text{otherwise} \end{cases} \tag{11}$$

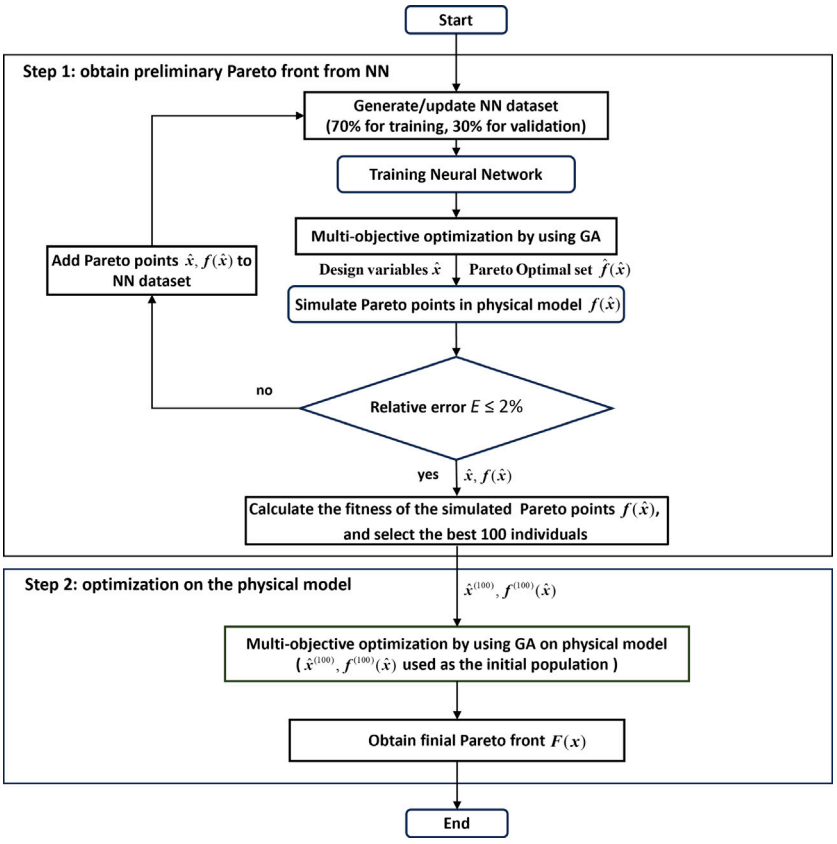

Fig. 8. Flow chart of the optimization procedure.

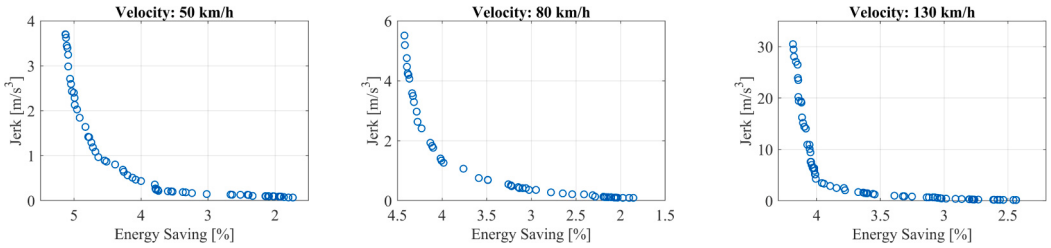

(a) Velocity: 50 km/h (b) Velocity: 80 km/h (c) Velocity: 130 km/h

Fig. 9. Pareto optimal sets for the three considered velocities.

Table 7
Energy consumption of the CS strategy.

Velocity [km/h]	Energy consumption [kWh/km]
50	0.1078
80	0.1524
130	0.2781

5.4. Optimization results

The described optimization procedure has been repeated for the three considered velocities (50 km/h, 80 km/h, and 130 km/h) and Fig. 9 shows the resulting Pareto optimal set in the objective functions domain. The energy saving is defined as the percentage reduction in energy consumption with respect to the CS strategy. Table 7 reports the fuel consumption of the CS strategy for the three considered velocities.

The depicted Pareto optimal sets show that the two objective functions, namely energy saving and maximum jerk, exhibit, as expected, a conflicting relationship. In the case of 130 km/h (Fig. 9(c)) a sharp change in the curvature appears on the Pareto optimal sets as the jerk approaches approximately 5 m/s^3. This curvature change is caused by the activation of the constraints on the rising interval t_2 and falling interval t_4. In accordance with the results reported in the literature (Li and Peng, 2012), the PnG strategy exhibits greater fuel savings with respect to the CS strategy at lower velocities. In fact, the maximum energy saving is about 5% at 50 km/h. Furthermore, the maximum jerk increases as the considered velocity increases.

According to Sohn et al. (2019), also the longitudinal acceleration delta, defined as the difference between the maximum acceleration and the minimum acceleration in a cycle, is related to longitudinal comfort. Thus, it is interesting to investigate the correlation between maximum jerk and the longitudinal acceleration delta of the optimal solutions. Table 8 shows the Spearman correlation coefficient (Press, 2007) between the maximum jerk and the longitudinal acceleration delta for the solutions belonging to the Pareto optimal sets.

At 50 and 80 km/h, the Spearman correlation coefficients is greater than 0.9, showing a clear direct correlation between the maximum jerk and the longitudinal acceleration delta. At 130 km/h, a smaller

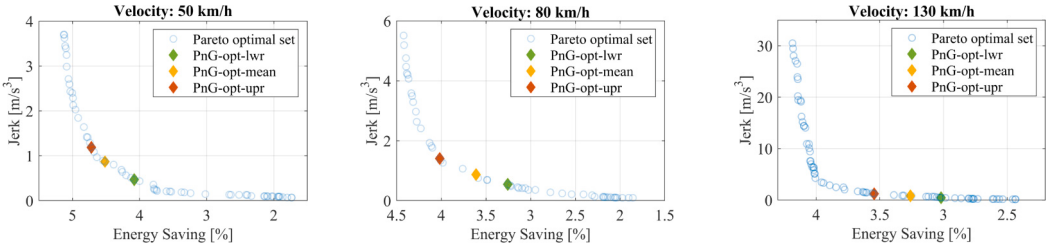

(a) Velocity: 50 km/h (b) Velocity: 80 km/h (c) Velocity: 130 km/h

Fig. 10. Optimal PnG strategies selected on the Pareto optimal set.

Table 8
Spearman correlation between the maximum jerk and the longitudinal acceleration delta for the computed solutions of the Pareto optimal sets.

	Velocity		
	50 km/h	80 km/h	130 km/h
Spearman correlation coefficient	0.9655	0.9352	0.7221

value of 0.72 has been found for the Spearman correlation coefficient. This value, however, indicates an overall positive correlation between maximum jerk and longitudinal acceleration delta.

6. Subjective evaluation of the optimal solutions

The Pareto optimal sets define sets of solutions that constitute the best compromise between conflicting objectives. However, these solutions are all equivalent, as none of them is dominated by any other solution. The designer has then to choose the preferred solution. In this section, we exploit the results of the experimental tests of Section 4 to identify three possible choices for each of the three velocities. Then, a new session of tests at the driving simulator is conducted to subjectively evaluate the selected solutions.

According to the definitions reported in Section 4.1, threshold 2 represents the limit between a comfortable and annoying level of jerk, which is highly related to the drivers' comfort preference. Therefore, for the three velocities, referring to the results in Section 4.4, the preferred solutions are chosen as the ones closest to the mean identified value of threshold 2 and the ones closest to this mean value plus and minus two times the standard deviation. The three selected solutions are labeled as "PnG-opt-mean", "PnG-opt-lwr" and "PnG-opt-upr", respectively for the mean value solution, the lower bound solution (mean minus two standard deviations) and the upper bound solution (mean plus two standard deviations). Fig. 10 and Table 9 show the selected solutions on the Pareto optimal set and their parameters.

The experimental evaluation of the chosen solution has been performed by using the same testing setup defined in Section 4. In particular, the same motion cueing parameters for the driving simulator are used.

For the tests, a panel of 12 participants has been considered. Of these participants, 7 also took part to the threshold estimation test and 5 additional participants are 3 males and 2 females (details in Table A.11). The tests have been performed approximately two weeks after the preliminary tests of Section 4. Participants have been asked to test the solutions starting from the velocity of 50 km/h to 130 km/h. For each vehicle velocity, the three optimal solutions were randomly tested, without informing the participants about the solution under test. Each solution has been tested once. After each test, for the considered solution, participants were asked if they would like to choose this driving strategy for long-distance traveling. Before the test, participants have been instructed about the possible answers and their qualitative description. Table 10 reports the possible answers and descriptions.

Fig. 11 displays the results of the subjective evaluation of the selected optimal solutions, indicating the frequency of selection for each answer. Consistent results are reported for all of the considered velocities, with the solutions at low levels of jerk felt as comfortable by most participants and only the solutions with high levels of jerk have been found uncomfortable by few participants.

Fig. 12 shows the results of the subjective evaluation of the optimal solutions in aggregated form. The evaluations have been aggregated by summing the answers for the three levels of jerk (lower bound, mean, and upper bound) at the different velocities. The figure shows a reduction in the perceived comfort as the level of jerk is increased. For the lower level, only in very few cases, the participants have found the proposed PnG strategies rather annoying, while the great majority of answers have considered these strategies as comfortable or overall comfortable. As the level of jerk increases, the number of answers describing as rather annoying the strategies increases and, for the highest level of jerk, in some cases strategies have been perceived as uncomfortable. These results can provide the designer indications on how to chose the preferred optimal PnG strategy. The mean value of the threshold is actually considered as comfortable or overall comfortable in the majority of the cases, but for a significant fraction of cases is felt as rather annoying. If the designer prefers to reduce this fraction, a level of jerk close to the lower bound of the identified threshold should be chosen, at the cost of a slight reduction of energy savings.

7. Conclusion

The paper presents a method for optimizing and validating PnG (Pulse and Glide) strategies for electric vehicles. The experimental validation was conducted by using a dynamic driving simulator, which provides a controlled and repeatable environment for safe testing.

As driving simulators are rarely used for evaluating longitudinal comfort, the first part of the paper has been devoted to defining a suitable testing procedure. Based on an analysis of similar tests in the literature aimed at defining longitudinal comfort using actual vehicles, longitudinal jerk has been identified as the most relevant metric. Preliminary tests, employing an up-down method, were conducted on the driving simulator to identify three jerk thresholds representing significant transitions in participants' perceptions. Additionally, this activity also provided supporting evidence of the correlation between the jerk responses obtained on the driving simulator and those reported in the literature obtained from experimental tests on real vehicles.

The first threshold corresponds to the jerk value at which participants felt the vehicle as comfortable but noticed a difference compared to a constant velocity ride. The second threshold aimed at identifying the jerk level at which participants no longer felt the vehicle as comfortable. Finally, the third threshold represented the jerk level at which the vehicle was deemed too uncomfortable to ride. Despite a limited number of testers were involved, preliminary results indicate that the identified jerk thresholds closely align with similar thresholds reported in the literature and identified through tests on actual vehicles. The standard deviation associated with these values is also comparable to

Table 9
Parameters of selected optimal solutions.

		t1	t2	t3	t4	t5	A	Average velocity [km/h]	Energy saving [%]	Max jerk [m/s^3]
50 km/h	PnG-opt-lwr	2.413	2.024	1.647	2.408	6.210	0.181	49.90	4.08	0.469
	PnG-opt-mean	2.376	0.998	3.266	1.281	7.674	0.168	49.92	4.52	0.869
	PnG-opt-upr	1.609	0.768	2.040	2.824	7.500	0.181	49.90	4.71	1.187
80 km/h	PnG-opt-lwr	2.898	2.392	1.723	2.671	5.237	0.309	79.93	3.27	0.547
	PnG-opt-mean	1.810	1.459	1.723	1.723	4.884	0.307	79.98	3.61	0.870
	PnG-opt-upr	1.810	1.109	1.723	1.723	4.977	0.316	79.91	3.79	1.141
130 km/h	PnG-opt-lwr	0.060	2.904	3.725	3.275	3.305	0.568	129.91	3.02	0.465
	PnG-opt-mean	0.060	1.799	3.569	1.565	3.197	0.564	129.94	3.26	0.824
	PnG-opt-upr	0.060	0.991	3.569	1.057	3.217	0.560	129.91	3.55	1.231

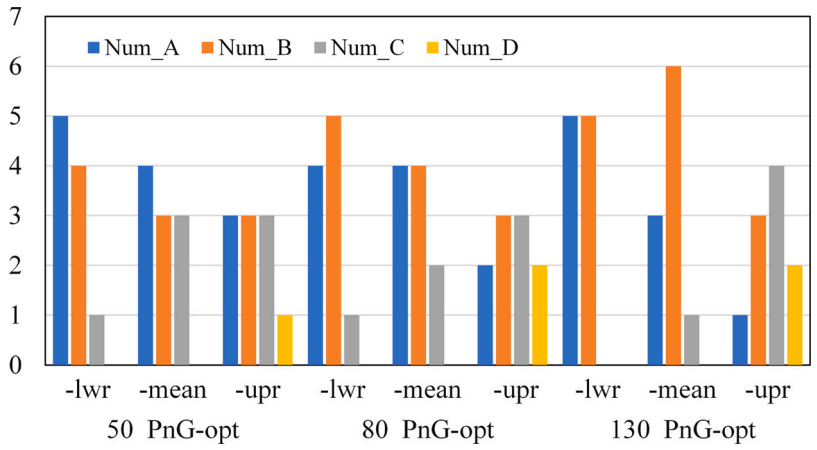

Fig. 11. Subjective test result for optimal PnG strategies. Definitions of answers A, B, C, and D in Table 10.

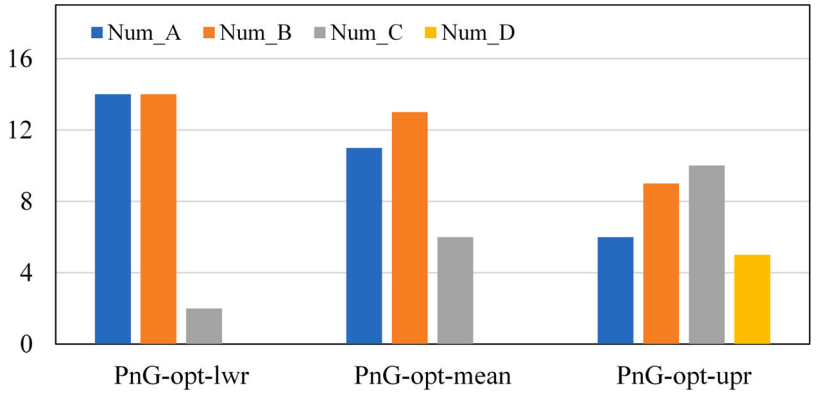

Fig. 12. Comprehensive evaluation of different jerk levels. Definitions of answers A, B, C, and D in Table 10.

Table 10
Qualitative description of the answers for the experimental evaluation of the chosen optimal solutions.

	Answer	Description
A	Yes	Comfortable, they would definitely travel with this strategy
B	More yes than no	A little bit annoying, but overall comfortable
C	More no than yes	Rather annoying, only travel with this strategy if there is no other option
D	No	Uncomfortable, they would not travel with this strategy

results reported in the literature. Additionally, the thresholds appear to be relatively independent on the longitudinal velocity of the vehicle. While further testing is needed to confirm these results, the size of the participant panel in the preliminary tests is comparable to that of similar tests in the literature.

The second part of the paper exploits the results of the preliminary tests to define a multi-objective optimization of PnG strategies for an electric vehicle. The Pareto optimal set, representing the best compromise between comfort and energy consumption, was derived through an offline optimization approach for three reference velocities, namely 50 km/h, 80 km/h, and 130 km/h, corresponding to urban roads, country roads, and motorway situations, respectively. Different PnG strategies were defined by modifying the accelerator actuation law, with comfort evaluated based on maximum jerk.

In the present study, the dynamic driving simulator demonstrated considerable potential for evaluating longitudinal ride comfort, particularly when assessing jerk-related effects within the Pulse-and-Glide (PnG) strategy. Objective jerk measurements obtained from the simulator were compared with reference data from a vehicle dynamics model, showing high accuracy in reproducing longitudinal jerk. Subjective

Table A.11
Participants' personal information.

	Gender	Age	Driving license	Duration of License Holding [years]	Driving Frequency	Experiment 1 (Section 4)	Experiment 2 (Section 6)
1	Male	53	Yes	35	Often	X	X
2	Male	37	Yes	19	Often	X	X
3	Female	28	Yes	9	Often	X	
4	Male	33	Yes	5	Often		X
5	Male	25	Yes	4	Often		X
6	Male	29	Yes	10	Normal	X	X
7	Male	32	Yes	14	Normal	X	X
8	Male	31	Yes	9	Normal	X	X
9	Male	33	Yes	5	Normal		X
10	Female	26	Yes	8	Normal		X
11	Female	31	Yes	7	Seldom	X	X
12	Male	32	Yes	10	Seldom	X	X
13	Female	29	Yes	4	Seldom		X

evaluations further confirmed a strong correlation with real vehicle experiences, supporting the simulator's effectiveness for comfort assessment. However, certain limitations should be noted. The PnG strategy used in this study involves frequent acceleration and deceleration with brief transition periods. Under these conditions, the dynamic driving simulator's longitudinal motion range proved sufficient to achieve highly accurate jerk reproduction, nearly at a 1:1 scale. In contrast, other driving scenarios involving prolonged acceleration and significant speed variations, or the use of simulators with a more limited longitudinal motion range, may require a reduced motion replication scale. In such cases, a decrease in the accuracy of comfort evaluations may occur.

The offline Pareto optimal set, which represents the best trade-offs between comfort and energy efficiency in accelerator commands, can be applied in real-time applications. These include serving as a reference for speed planning in autonomous vehicles (AVs), vehicle platoon control, or as a look-up table that allows the controller to offer multiple selectable options based on the driver's preferences. Additionally, the proposed methodology can be extended to investigate comfort-oriented driving under varying traffic conditions by incorporating relevant constraints. In particular, the second threshold, the critical value between comfortable and annoying level of jerk, is highly related to the drivers' comfort preference. Three Pareto points of each considered reference velocities were therefore chosen at a jerk level corresponding to the second threshold and tested by a panel of participants, including those from the preliminary tests. These tests showed consistent results compared to the preliminary tests, demonstrating appreciable differences between the various levels of jerk of the chosen optimal solutions. It emphasizes the role of the Pareto optimal set in offering adaptable solutions and indicates that dynamic driving simulators can effectively be used for assessing the longitudinal comfort of vehicles and developing PnG strategies

CRediT authorship contribution statement

Haoxiang Xue: Writing – original draft, Visualization, Validation, Software, Investigation, Data curation. **Federico Maria Ballo:** Writing – review & editing, Validation, Methodology, Investigation, Formal analysis, Data curation. **Giorgio Previati:** Writing – review & editing, Supervision, Methodology, Investigation, Formal analysis, Conceptualization. **Gianpiero Mastinu:** Writing – review & editing, Supervision, Methodology, Funding acquisition, Conceptualization. **Massimiliano Gobbi:** Writing – review & editing, Supervision, Methodology, Funding acquisition, Conceptualization.

Declaration of competing interest

The authors declare the following financial interests/personal relationships which may be considered as potential competing interests: Massimiliano Gobbi reports financial support was provided by European Union - NextGeneratonEU. Haoxiang Xue reports financial support was provided by China Scholarship Council. If there are other authors, they declare that they have no known competing financial interests or personal relationships that could have appeared to influence the work reported in this paper.

Acknowledgments

The research activities have been funded by the European Union as part of NextGenerationEU, M4C2 I1.1, Project PRIN 2022 "HL4IT", Prot. 2022L3M25K – CUP D53D23003750006. The author, Haoxiang Xue, would like to thank the China Scholarship Council for the financial support (CSC, No. 202006050042). This manuscript reflects only the authors views and opinions, neither the European Union nor the European Commission can be considered responsible for them.

Appendix. PArticipants

Driving frequency is defined as follows.

- Often: above 10000 km/year
- Normal: 3000 km/year to 10000 km/year
- Seldom: below 3000 km/year

All participants signed an informed consent, a privacy statement in compliance with European GDPR 679/2016, and the research has been approved by the Ethical Committee of Politecnico di Milano under "Parere n. 16/2023" (ethical approval).

Data availability

Data will be made available on request.

References

Aledhari, M., Rahouti, M., Qadir, J., Qolomany, B., Guizani, M., Al-Fuqaha, A., 2023. Motion comfort optimization for autonomous vehicles: Concepts, methods, and techniques. IEEE Internet Things J..

Aramrattana, M., Habibovic, A., Englund, C., 2021. Safety and experience of other drivers while interacting with automated vehicle platoons. Transp. Res. Interdiscip. Perspect. (ISSN: 2590-1982) 10, 100381. http://dx.doi.org/10.1016/j.trip.2021.100381, URL: https://www.sciencedirect.com/science/article/pii/S2590198221000889.

Arconada, V.S., García-Barruetabeña, J., Haas, R., 2023. Validation of a ride comfort simulation strategy on an electric Stewart platform for real road driving applications. J. Low Freq. Noise Vib. Act. Control. 42 (1), 368–391.

Bae, I., Moon, J., Jhung, J., Suk, H., Kim, T., Park, H., Cha, J., Kim, J., Kim, D., Kim, S., 2020. Self-driving like a human driver instead of a robocar: Personalized comfortable driving experience for autonomous vehicles. arXiv preprint arXiv:2001.03908.

Bae, I., Moon, J., Seo, J., 2019. Toward a comfortable driving experience for a self-driving shuttle bus. Electronics 8 (9), 943.

Ballo, F., Stabile, P., Gobbi, M., Mastinu, G., 2022. A lightweight ultra-efficient electric vehicle multi-physics modeling and driving strategy optimization. IEEE Trans. Veh. Technol. 71 (8), 8089–8103. http://dx.doi.org/10.1109/TVT.2022.3172174.

Bruck, L., Haycock, B., Emadi, A., 2020. A review of driving simulation technology and applications. IEEE Open J. Veh. Technol. 2, 1–16.

Bruschetta, M., Maran, F., Beghi, A., 2017. A nonlinear, MPC-based motion cueing algorithm for a high-performance, nine-DOF dynamic simulator platform. IEEE Trans. Control Syst. Technol. 25 (2), 686–694. http://dx.doi.org/10.1109/TCST.2016.2560120.

Chada, S.K., Görges, D., Ebert, A., Teutsch, R., Subramanya, S.P., 2023. Evaluation of the driving performance and user acceptance of a predictive eco-driving assistance system for electric vehicles. Transp. Res. Part C: Emerg. Technol. 153, 104193.

de Winkel, K.N., Irmak, T., Happee, R., Shyrokau, B., 2023. Standards for passenger comfort in automated vehicles: Acceleration and jerk. Appl. Ergon. 106, 103881.

Dombi, J., Gera, Z., 2005. The approximation of piecewise linear membership functions and Łukasiewicz operators. Fuzzy Sets and Systems (ISSN: 01650114) 154 (2), 275–286. http://dx.doi.org/10.1016/j.fss.2005.02.016.

DriSMi, 2025. Driving simulator, politecnico di milano. [Online]. https://www.drismi.polimi.it/the-driving-simulator/.

El hamdani, S., Bouchner, P., Kunclova, T., Toman, P., Svoboda, J., Novotnỳ, S., 2023. Fidelity assessment of motion platform cueing: Comparison of driving behavior under various motion levels. Sensors 23 (12), 5428.

Faria, M., Duarte, G., Baptista, P., 2019. Assessing electric mobility feasibility based on naturalistic driving data. J. Clean. Prod. (ISSN: 0959-6526) 206, 646–660. http://dx.doi.org/10.1016/J.JCLEPRO.2018.09.217.

Faria, R., Moura, P., Delgado, J., De Almeida, A.T., 2012. A sustainability assessment of electric vehicles as a personal mobility system. Energy Convers. Manage. 61, 19–30. http://dx.doi.org/10.1016/j.enconman.2012.02.023.

Fisher, D.L., Rizzo, M., Caird, J., Lee, J.D., 2011. Handbook of driving simulation for engineering, medicine, and psychology. CRC Press.

Gobbi, M., 2013. A k, k-ϵ optimality selection based multi objective genetic algorithm with applications to vehicle engineering. Optim. Eng. 14 (2), 345–360. http://dx.doi.org/10.1007/s11081-011-9185-8.

Gobbi, M., Mastinu, G., Pennati, M., Previati, G., 2014. InTenso+ System: Measured Centre of Gravity Locations and Inertia Tensors of Road Vehicles. In: Vol. 3 16th Int. Conf. Adv. Veh. Technol. 11th Int. Conf. Des. Educ. 7th Front. Biomed. Devices. American Society of Mechanical Engineers, http://dx.doi.org/10.1115/DETC2014-34300, V003T01A037.

Gouribhatla, R., Pulugurtha, S.S., 2022. Drivers' behavior when driving vehicles with or without advanced driver assistance systems: A driver simulator-based study. Transp. Res. Interdiscip. Perspect. (ISSN: 2590-1982) 13, 100545. http://dx.doi.org/10.1016/j.trip.2022.100545, URL: https://www.sciencedirect.com/science/article/pii/S2590198222000094.

Hayafune, K., Yoshida, H., 1990. Control method of autonomous vehicle considering compatibility of riding comfort and vehicle controllability. Technical Report, SAE Technical Paper.

Heißing, B., Ersoy, M., 2010. Chassis handbook: fundamentals, driving dynamics, components, mechatronics, perspectives. Springer Science & Business Media.

Hoberock, L.L., 1976. A survey of longitudinal acceleration comfort studies in ground transportation vehicles. Technical Paper, Council for Advanced Transportation Studies.

Huang, Q., Wang, H., 2004. Fundamental study of jerk: evaluation of shift quality and ride comfort. Technical Report, SAE Technical Paper.

Hubbard, G.A., Youcef-Toumi, K., 1997. System level control of a hybrid-electric vehicle drivetrain. In: Proceedings of the 1997 American Control Conference (Cat. No. 97CH36041), vol. 1, IEEE, pp. 641–645.

ISO 15622:2018(E), 2018. Intelligent transport systems - Adaptive cruise control systems — Performance requirements and test procedures. International Organization for Standardization, Geneva, CH.

Jungblut, E., Grube, T., Linssen, J., Stolten, D., 2023. Fuel-saving opportunities for automated vehicles: A driving cycle analysis. Transp. Res. Interdiscip. Perspect. (ISSN: 2590-1982) 22, 100964. http://dx.doi.org/10.1016/j.trip.2023.100964, URL: https://www.sciencedirect.com/science/article/pii/S2590198223002117.

Kim, J., Ahn, C., 2019. Real-time speed trajectory planning for minimum fuel consumption of a ground vehicle. IEEE Trans. Intell. Transp. Syst. 21 (6), 2324–2338.

Lee, J., 2009. Vehicle Inertia Impact on Fuel Consumption of Conventional and Hybrid Electric Vehicles Using Acceleration and Coast Driving Strategy (Ph.D. thesis). Virginia Tech.

Levitt, H., 1971. Transformed up-down methods in psychoacoustics. J. Acoust. Soc. Am. 49 (2B), 467–477.

Li, S.E., Peng, H., 2012. Strategies to minimize the fuel consumption of passenger cars during car-following scenarios. Proc. Inst. Mech. Eng. Part D: J. Automob. Eng. 226 (3), 419–429. http://dx.doi.org/10.1177/0954407011420214.

Martin, D., Litwhiler, D., 2008. An investigation of acceleration and jerk profiles of public transportation vehicles. In: 2008 Annual Conference & Exposition. pp. 13–194.

Mastinu, G., Gobbi, M., Miano, C., 2007. Optimal Design of Complex Mechanical Systems: With Applications to Vehicle Engineering. Springer Science & Business Media.

Melzi, S., Previati, G., 2024. Driving simulator: Analysing the impact of mechanical latency on the perception of lateral dynamics. J. Vib. Control http://dx.doi.org/10.1177/10775463241246906.

Momen, F., Rahman, K.M., Son, Y., Savagian, P., 2016. Electric motor design of general motors' Chevrolet Bolt electric vehicle. SAE Int. J. Altern. Powertrains 5 (2), 286–293. http://dx.doi.org/10.4271/2016-01-1228.

Muehlbacher, D., Will, S., Merkel, N., Perterer, N., Mlakar, S., Haller, M., Perterer, M., 2023. Compliance to eco-riding recommendations on an E-scooter: Effects on energy consumption and user acceptance. Transp. Res. Interdiscip. Perspect. (ISSN: 2590-1982) 20, 100831. http://dx.doi.org/10.1016/j.trip.2023.100831, URL: https://www.sciencedirect.com/science/article/pii/S2590198223000787.

Mussone, L., 2023. Assessing the effects of road geometry and fidelity on driver behaviour in driving simulator experiments. Transp. Res. Interdiscip. Perspect. (ISSN: 2590-1982) 20, 100835. http://dx.doi.org/10.1016/j.trip.2023.100835, URL: https://www.sciencedirect.com/science/article/pii/S2590198223000829.

Nandi, A.K., Chakraborty, D., Vaz, W., 2015. Design of a comfortable optimal driving strategy for electric vehicles using multi-objective optimization. J. Power Sources 283, 1–18.

Olivier, J.-C., Wasselynck, G., Chevalier, S., Auvity, B., Josset, C., Trichet, D., Squadrito, G., Bernard, N., 2017. Multiphysics modeling and optimization of the driving strategy of a light duty fuel cell vehicle. Int. J. Hydrog. Energy 42 (43), 26943–26955. http://dx.doi.org/10.1016/j.ijhydene.2017.06.243.

Orlovska, J., Novakazi, F., ard Lars-Ola, B., Karlsson, M., Wickman, C., Söderberg, R., 2020. Effects of the driving context on the usage of automated driver assistance systems (ADAS) -naturalistic driving study for ADAS evaluation. Transp. Res. Interdiscip. Perspect. (ISSN: 2590-1982) 4, 100093. http://dx.doi.org/10.1016/j.trip.2020.100093, URL: https://www.sciencedirect.com/science/article/pii/S259019822030004X.

Papalambros, P.Y., Wilde, D.J., 2000. Principles of optimal design. Modeling and computation. Cambridge Universirìty Press.

Parsons, K., Griffin, M., 1988. Whole-body vibration perception thresholds. J. Sound Vib. 121 (2), 237–258.

Peng, C., Carlowitz, S., Madigan, R., Marberger, C., Lee, J.D., Krems, J., Beggiato, M., Romano, R., Wei, C., Wooldridge, E., Happee, R., Hagenzieker, M., Merat, N., 2024. Conceptualising user comfort in automated driving: Findings from an expert group workshop. Transp. Res. Interdiscip. Perspect. (ISSN: 2590-1982) 24, 101070. http://dx.doi.org/10.1016/j.trip.2024.101070, URL: https://www.sciencedirect.com/science/article/pii/S2590198224000563.

Peng, C., Wei, C., Solernou, A., Hagenzieker, M., Merat, N., 2025. User comfort and naturalness of automated driving: The effect of vehicle kinematic and proxemic factors on subjective response. Appl. Ergon. 122, 104397.

Plöchl, M., Edelmann, J., 2007. Driver models in automobile dynamics application. Veh. Syst. Dyn. 45 (7–8), 699–741.

Press, W.H., 2007. Numerical Recipes 3rd Edition: the Art of Scientific Computing. Cambridge University Press.

Sareni, B., Krahenbuhl, L., 1998. Fitness sharing and niching methods revisited. IEEE Trans. Evol. Comput. 2 (3), 97–106. http://dx.doi.org/10.1109/4235.735432.

Sekar, R., Jacome, O., Chrstos, J.P., Stockar, S., 2022. Statistical assessment of driving behavior on simulators during naturalistic driving. pp. 73–76,

Shieh, S.-Y., Ersal, T., Peng, H., 2023. Pulse-and-glide operations for hybrid electric vehicles in the car-following scenario. IEEE Trans. Veh. Technol..

Smyth, J., Jennings, P., Mouzakitis, A., Birrell, S., 2018. Too sick to drive: How motion sickness severity impacts human performance. In: 2018 21st International Conference on Intelligent Transportation Systems. ITSC, IEEE, pp. 1787–1793.

Sohn, C., Andert, J., Jolovic, D., 2020. An analysis of the tradeoff between fuel consumption and ride comfort for the pulse and glide driving strategy. IEEE Trans. Veh. Technol. 69 (7), 7223–7233. http://dx.doi.org/10.1109/TVT.2020.2994467.

Sohn, C., Andert, J., Manfouo, R.N.N., 2019. A driveability study on automated longitudinal vehicle control. IEEE Trans. Intell. Transp. Syst. 21 (8), 3273–3280. http://dx.doi.org/10.1109/TITS.2019.2925193.

Soranzo, A., Grassi, M., 2014. PsychoacoUStics: a comprehensive MATLAB toolbox for auditory testing. Front. Psychol. 5, 712.

Stabile, P., Ballo, F., Mastinu, G., Gobbi, M., 2021. An Ultra-Efficient Lightweight Electric Vehicle-Power Demand Analysis to Enable Lightweight Construction. Energies (ISSN: 1996-1073) 14 (3), 766. http://dx.doi.org/10.3390/en14030766, URL: https://www.mdpi.com/1996-1073/14/3/766.

Stabile, P., Ballo, F., Previati, G., Mastinu, G., Gobbi, M., 2023. Eco-driving strategy implementation for ultra-efficient lightweight electric vehicles in realistic driving scenarios. Energies 16 (3), 1394.

Steimle, M., Stange, V., Vollrath, M., Maurer, M., 2025. Human&vehicle-in-the-loop test method in human factors research on automated vehicles: Conceptualization, realization, case-study, and lessons learned. Transp. Res. Interdiscip. Perspect. (ISSN: 2590-1982) 29, 101282. http://dx.doi.org/10.1016/j.trip.2024.101282, URL: https://www.sciencedirect.com/science/article/pii/S2590198224002689.

Targosz, M., Skarka, W., Przystałka, P., 2018. Model-based optimization of velocity strategy for lightweight electric racing cars. J. Adv. Transp. 2018, http://dx.doi.org/10.1155/2018/3614025.

VI-grade GmbH, 2021. VI-grade. VI-CarRealTime 2021.3 documentation. Darmstadt, Germany.

VI-grade GmbH, 2022. VI-grade. VI-Drivesim 2022.2 documentation. Darmstadt, Germany.

Wu, D., Zhu, B., Tan, D., Zhang, N., Gu, J., 2019. Multi-objective optimization strategy of adaptive cruise control considering regenerative energy. Proc. Inst. Mech. Eng. Part D: J. Automob. Eng. 233 (14), 3630–3645.

www.evspecifications.com, 2020. Chevrolet Bolt EV - Specification and price. [Online]. https://www.evspecifications.com/en/model/0545d6/.

Xu, S., Li, S.E., Zhang, X., Cheng, B., Peng, H., 2015. Fuel-optimal cruising strategy for road vehicles with step-gear mechanical transmission. IEEE Trans. Intell. Transp. Syst. 16 (6), 3496–3507.

Xue, H., Ballo, F., Previati, G., Gobbi, M., 2024. Eco-driving of electric vehicles - objective and subjective evaluation of passenger comfort by a dynamic driving simulator. IEEE Trans. Veh. Technol. 555–577. http://dx.doi.org/10.1109/TVT.2024.3461166.

Xue, H., Previati, G., Gobbi, M., Mastinu, G., 2023. Research and development on noise, vibration, and harshness of road vehicles using driving simulators–a review. SAE Int. J. Veh. Dyn. Stab. NVH 7 (4), 555–577.

Zhao, L., Nybacka, M., Drugge, L., Rothhämel, M., Habibovic, A., Hvitfeldt, H., 2024. The influence of motion-cueing, sound and vibration feedback on driving behavior and experience – a virtual teleoperation experiment. IEEE Trans. Intell. Transp. Syst..

Zhu, W., Zhang, X., Hu, C., Zhao, B., Peng, S., Yang, H., 2022. A comfort quantification method based on semi-supervised learning for automated vehicle at lane change scenarios. IEEE Trans. Intell. Veh..